Intermittency reinjection probability density function with and without noise effects

SERGIO ELASKAR
Universidad Nacional de Córdoba and CONICET
Department of Aeronautics
Av. Velez Sarfield 1611, 5000 Cordoba
ARGENTINA
sergio.elaskar@gmail.com

EZEQUIEL DEL RIO
Universidad Politécnica de Madrid
Department of Applied Physics, ETSIA
Plaza Cardenal Cisneros 3, Madrid
SPAIN
ezequiel.delrio@upm.es

Abstract: Intermittency phenomenon is a continuous route from regular to chaotic behaviour. Intermittency is an occurrence of a signal that alternates chaotic bursts between quasi-regular periods called laminar phases, driven by the so called reinjection probability density function (RPD). In this paper is introduced a new technique to obtain the RPD for type-II and III intermittency. The new RPD is more general than the classical one and includes the classical RPD as a particular case. The probabilities of the laminar length, the average laminar lengths and the characteristic relations are determined with and without lower bound of the reinjection in agreement with numerical simulations. Finally, it is analyzed the noise effect in intermittency. A method to obtain the noisy RPD is developed extending the procedure used in the noiseless case. The analytical results show a good agreement with numerical simulations.

Key–Words: Intermittency, chaos, noise.

1 Introduction

Intermittency is a particular route to chaos, where a transition between regular or laminar and chaotic phases occur. Pomeau and Maneville introduced the concept of intermittency in [1, 2]. The intermittency phenomenon has been observed in several physical topics such as Lorenz system, Rayleigh-Bénard convection, forced nonlinear oscillators, plasma physics, turbulence, etc. Also, it is very important to properly characterise the intermittency phenomenon, especially in those fields, whose exact governing equations are partially unknown, as it happens in economical and medical sciences [3, 4]. Traditionally, intermittency is calssified into three differents types called I, II and III [5, 6] according to the Floquet multipliers or eigenvalue in the local Poincaré map. By means of Poincaré sections it is possible to study the intermittency mechanism using maps. Intermittency type-II begins in a subcritical Hopf bifurcation or Naimark-Sacker bifurcation [7], therefore, two complex-conjugate Floquet multipliers or two complex-conjugate eigenvalues of the local Poincaré map exit the unit circle. Type-III intermittency is related to a subcritical period-doubling or flip bifurcation when one Floquet multiplier leaves the unit circle through -1. In the intermittency phenomenon, when a control parameter exceeds a threshold value, the system behaviour changes abruptly to a larger attractor by means an explosive bifurcation [6]. Then, the periodic orbit becames chaotic. Concerning to type-I intermittency, we have preparing an extension of the methodology shown in this paper for type-II and type-III. Then, in all the cases, a fixed point of the local Poincaré map becomes unstable for positive values of a control parameter ε. The local Poincaré maps for type-I, type-II and type-III intermittencies are respectively given by: $x_{n+1} = \varepsilon + x_n + a\ x_n^2$, $x_{n+1} = (1+\varepsilon)x_n + a\ x_n^3$ and $x_{n+1} = -(1+\varepsilon)\ x_n - a\ x_n^3$, where ε and a must be higher than 0. However, to generate intermittency it is necessary to have a reinjection mechanism that maps back from the chaotic zone into the local regular or laminar one. This mechanism is described by the so called reinjection probability density function (RPD) close to the unstable point, which is determined by the non linear dynamics of the system itself. Therefore, the accurate evaluation of the RPD function is extremely important to correctly analize and describe the intermittency phenomenon. It is important to note that in only a few cases it is possible to obtain an analytical expression for the RPD function. Also, it is not a simple task to experimentally or numerically obtain the RPD due to the huge amount of data needed. Besides this, the statistical fluctuations induced in the numerical computations and the experimental measurements are difficult to be estimated. For theses reasons several different

ISBN: 978-1-61804-131-9

approaches have been used to describe the RPD for the intermittent systems. The most popular approach used is to consider the RPD as a constant, that is uniform reinjection. However, different approaches have been implemented. Some of them are built using a characteristic of the particular non-linear proccesses. Nevertheless, these RPD functions can not be applied for other systems. For instance, to investigate the effect of noise in type-I intermittency, sometimes it is assumed that the reinjection is localized in a fixed point [8]. For type-III intermittency in an electronic circuit the RPD was considered as proportional to $1/\sqrt{x-\Delta}$ in [9]. The previous examples show that there is no efficient method to obtain the RPD function. However, recently a more general RPD that includes the uniform reinjection as a particular case has been introduced [10, 11]. In this paper we present a complete description of the new formulation for two intermittency types. The formulation includes the lower bound of the reinjection concept (LBR), and permits the calculation of the laminar length statistic and the characteristic relations. Finally we analize the influence of the noise in the new theory [12].

2 Formulation for the RPD function

In this section we briefly describe the theoretical framework that accounts for a wide class of dynamical systems exhibiting intermittency. We consider a general one-dimensional map: $x_{n+1} = F(x_n)$. The RPD function, denoted here by $\phi(x)$, specifies the statistical behavior of the reinjection trajectories and it depends on the specific form of $F(x)$. We note that there is not a general scheme or methodology to obtain the RPD function from experimental or numerical data. Therefore a formulation allowing the evaluation of the RPD function will be useful. The main concept to reach a more general formulation is given by the following integral [10]:

$$M(x) = \begin{cases} \frac{\int_{x_s}^{x} \tau\ \phi(\tau)\ d\tau}{\int_{x_s}^{x} \phi(\tau)\ d\tau} & \text{if } \int_{x_s}^{x} \phi(\tau) d\tau \neq 0 \\ 0 & \text{otherwise} \end{cases} \tag{1}$$

where x_s is a "starting" point, $x_s \leq x \leq c$, and c is a constant verifying $c > 0$ and it specifies the limits of the laminar region around of the vanished fixed point x_0. Therefore, the laminar zone of intermittency is defined by $[-c + x_0; x_0 + c]$. In the previous work [10] we used $x_s = x_0$; however, a more general approach considering x_s different to x_0 was established in [11]. We note that the integral $M(x)$ smooths the experimental o numerical data series, and its numerical estimation is more robust than the direct evaluation of the function $\phi(x)$. As the function $M(x)$ is an average over the reinjection points in the laminar interval, we can calculate it as:

$$M(x) \approx \frac{1}{n} \sum_{j=1}^{n} x_j, \qquad x_{n-1} < x \leq x_n \tag{2}$$

where the data set (reinjection points) $\{x_j\}_{j=1}^{N}$ must be sorted from lowest to highest, i.e. $x_j \leq x_{j+1}$. For a wide class of maps exhibiting intermittency, the function $M(x)$ satisfies a linear approximation:

$$M(x) = \begin{cases} m(x - \hat{x}) + \hat{x} & \text{if } \ x \geq \hat{x} \\ 0 & \text{otherwise} \end{cases} \tag{3}$$

where the slope $m \in (0, 1)$ is a free parameter, and $\hat{x}$ is the lower boundary of the reinjection. Then, using Eqs.(1 and 3) we can obtain the corresponding RPD:

$$\phi(x) = \lambda(x - \hat{x})^{\alpha}, \quad \text{with} \quad \alpha = \frac{2m - 1}{1 - m} \tag{4}$$

where λ is a normalization constant. We can note that for $m = 1/2$ we recover the most implemented approach that uses the uniform RPD.

3 Type-II Intermittency

In this section we applied the new formulation to an illustrating one-dimensional map presenting type-II intermittency, and closely following previously published work [10]. The implemented map has allowed us to analyze different types of the reinjection mechanism:

$$x_{n+1} = \begin{cases} F(x_n) & x_n \leq x_r \\ (F(x_n) - 1)^{\gamma} & x_n > x_r \end{cases} \tag{5}$$

where $F(x) = (1+\varepsilon)x_n + (1-\varepsilon)x_n^p$, x_r is defined by $F(x_r) = 1$, and ε is the control parameter. The origin of the map $x = 0$ is always a fixed point, however it is only stable for $-2 < \varepsilon < 0$. For $\varepsilon > 0$ the fixed point is unstable. The iterated points x_n of an inicial point, close to the origin, increases due to a process governed by parameters ε and p. A chaotic burst happens if x_n becomes larger than x_r; this chaotic process will be finished when x_n is reinjected into the laminar zone. From this reinjected point, a new iterative process governed by ε and p will cause an increase of the iterative points. We note that γ drives the reinjection mechanism, whereas p and ε influence the laminar phase duration. If we use $\gamma = 1$ and $p = 2$ in Eq.(5), we recover the map used by Manneville in his pioneer paper [13]. If we use $p = 3$, the local form of the map corresponds with the local Poincare map of type-II intermittency. We have numerically

evaluated the function $M(x)$ obtaining, in approximation, the following linear form $M(x) = mx$. Figure (1) shows numerical evaluations of $M(x)$ for different values of parameter γ together with the corresponding least squares straight line fitting. Always we find that $|m| < 1$. We have used the following parameters: in the upper line $\gamma = 2$ and $\varepsilon = 10^{-3}$, and for the lower line $\gamma = 0.65$ and $\varepsilon = 10^{-4}$. According to previous results, we consider that the function M is linear, $M(x) = mx$. Then the RPD can be expressed by Eq.(4) with $\lambda = \frac{\alpha+1}{c^{\alpha+1}}$. Note that $\phi(x)$ is determined only by the parameter m, which is easier to measure than the complete function $\phi(x)$. Note that the shape of $\phi(x)$ can be very different from the flat line (uniform reinjection), for instance $\lim_{x\to 0}\phi(x)$ is infinity when $0 < m < 1/2$ and zero if $1/2 < m < 1$. In Fig.(2) points indicate the numerical RPD functions, and the theoretical functions for $\phi(x)$ given by Eq.(4) are represented by continuous lines. We are considering the same two cases shown in Fig.(1). We can observe that the numerical data and theoretical results have a very good agreement. Note that the continuous

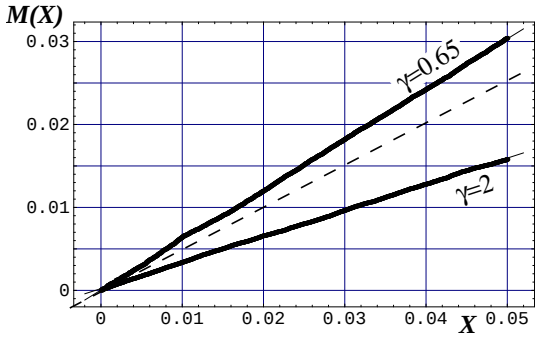

Figure 1: Function $M(x)$ for the map (5) with $p = 3$. Continuous lines show the linear fit of the numerical data. The slope of the dashed line is 0.5. In the upper line $\gamma = 2$ and $\varepsilon = 10^{-3}$ whereas for the lower case $\gamma = 0.65$ and $\varepsilon = 10^{-4}$

curve reduces the statistical fluctations of the numerical data. We observe that the slope m determines the value of the exponent α in the reinjection function (4), hence it rules the reinjection mechanism and it has direct influence in the the length probability density, the average laminar length and the characteristic relation. The density of the laminar lengths probability $\phi_l(l)$ is a global property and it is related to $\phi(l, c)$ [10, 11]:

$$\phi_l(l,c) = \lambda \left(\frac{\varepsilon}{\left(a + \frac{\varepsilon}{c^{(p-1)}}\right) e^{(p-1)\varepsilon l} - a} \right)^{\frac{p+\alpha}{p-1}} \times \times \left(a + \frac{\varepsilon}{c^{(p-1)}}\right) e^{(p-1)\varepsilon l} \quad (6)$$

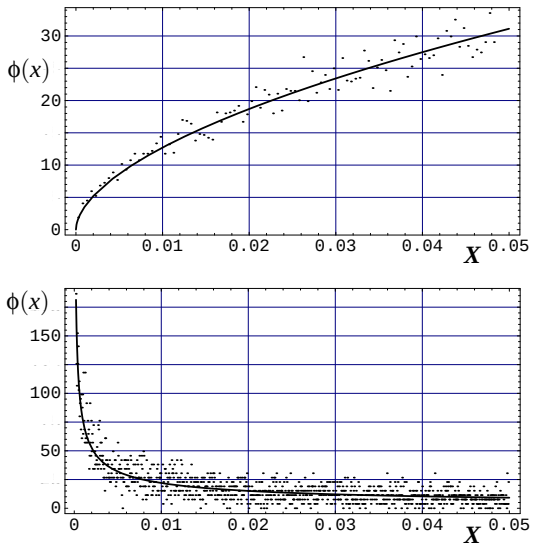

Figure 2: RPD for map (5). Upper and lower pictures correspond with the upper and lower lines of Fig.(1) respectively. Dots indicate numerical evaluations and continuous lines show the analytival results.

We can note that $\phi_l(l, c)$ depends on the global parameter α. Hence, the probability of the laminar length is determined by the slope m of the function $M(x)$. Fig.(3) shows a comparisson between the analytical results calculated using Eq.(6) with the numerical results for the map (5). We can observe a good agreement between numerical data and the theoretical results. Another important property of the intermittent

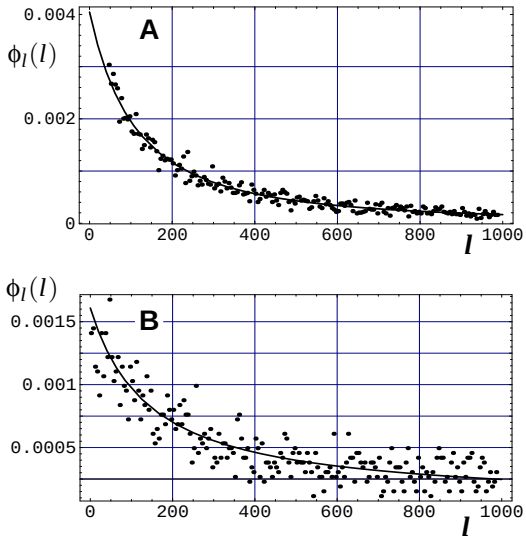

Figure 3: ϕ_l for map (5) using the same parametres that as Fig.(1).

behaviour is the average laminar length $\bar{l}$, that if m

does not depend on ε, can be written as [10]:

$$\bar{l} \approx \frac{1}{ac^{\alpha+1}} \left(\frac{a}{\varepsilon}\right)^{\frac{p-\alpha-2}{p-1}} \frac{\pi}{p-1} \sin^{-1}\left(\frac{\pi(1+\alpha)}{p-1}\right) \tag{7}$$

so the characteristic relation can be writte as:

$$\bar{l} \propto \varepsilon^{\frac{\alpha+2-p}{p-1}} \tag{8}$$

The characteristic relation depends on both: the behavior of the local map around the fixed point, and on the global dynamic of the map represented by the parameters α or m. The map (5), in the region where the chaotic dynamic occurs, depends on the exponent γ, so we expect that the RPD also will depend on γ. Then, we expect that α and m will be strongly dependent on γ and weakly on parameters ε. We evaluate $\bar{l}$ for several values of γ as the values of ε change. The results are shown in Fig.(4) for different values of γ and p. In Fig.(4) four lines are plotted, the three

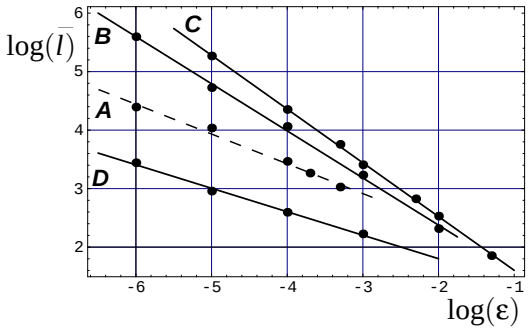

Figure 4: Characteristic relation for different γ in the map (5). Dots shows numerical data and lines show the least squares straight fitting. For lines A, B and C, p is 3 and γ is 1, 2 and 3 for case A, B and C respectively. For line D are $p = 2$ and $\gamma = 1.5$.

upper lines (A, B and C) show numerical and theoretical results for $p = 3$ in Eq.(5). The analytical expresion for the characteristic relation is given by Eq.(8), then we expected that the slopes of lines A, B and C are the exponents of the characteristic relation to $p = 3$. The value of m is obtained for each point of the Fig.(4) using the function $M(x)$, and this value is almost constant for each line of the figure as follows: $m_A \approx 0.49, m_B \approx 0.32, m_C \approx 0.22$. Hence the expected slopes for lines A, B and C are respectively: $slope_A \approx -0.51, slope_B \approx -0.77, slope_C \approx -0.86$. On the other hand, if we fit the numerical data, represented by points, in Fig.(4) we obtain the following slopes -0.51, -0.80 and -0.92 for lines A,B and C respectively. These results are in agreement with the expected ones.

4 Type-III Intermittency

In this section we used the function $M(x)$ to to study the RPD in the type-III intermittency. A more detailed description of this method can be found in [11]. For one-dimensional map presenting type III-intermittency, the Schwartzian derivative must be positive at the critical point [14]. Type-III intermittency was observed for the first time in the Bénard convection in a rectangular cell [16]. In this reference the Poincaré map presents a gap without reinjection around the neighborhood of the unstable fixed point. This behavior suggests that exists a lower bound of the reinjection (LBR). Here, we will extend the results obtained in the previous section to type-III intermittency to obtain a complete description of the laminar length statistic and the effect of the LBR. To do this we introduce the illustrating map:

$$\begin{aligned} x_{n+1} = F(x_n) = -(1+\varepsilon)\, x_n - a\, x_n^3 + \\ + b\, x_n^6\, \sin(x_n) \quad \text{with} \quad a > 0 \end{aligned} \tag{9}$$

where $x = 0$ is a fixed point of the map. This fixed point is asymptotically stable when ε satisfies $-2 < \varepsilon < 0$, and it is unstable for $\varepsilon > 0$ and the Schwartzian derivative $SF(x)$ is positive. For points far enough from the unstable point, the last term in Eq.(9) provides an efficient mechanism for reinjection. The non-linear behavior of the Eq.(9) is completely different from the non-linear behavior of the map used for type-II intermittency. Therefore, with the map (9) we not only study type-III intermittency, but we also extend the new formulation to another wide set of maps. The reinjection mechanism depends on the value of $F(x_r)$ at extreme points x_r. As n increases, any point x_n close to the origin distances itself in a process driven by the parameters ε and a in the cubic term of the map. For large n, the influence of the RHS third term in Eq.(9) increases and x_n approaches a x_r point giving rise the reinjection mechanism into the laminar zone. There is no reinjection around the unstable fixed point for $b > b_C \simeq 1.07$ [11]. The LBR is defined by the closest reinjection point of the fixed point [15]. However, there are no LBR if $b < b_c$ for the same values of a and ε. Fig.(5) plots the function $M(x)$ calculated using the map (9) for $a = 1$ and $\varepsilon = 0.01$. In this figure there are two curves calculated using two different values of the parameter b. Both curves $M(x)$ can be approximated by straight lines, hence according with Eq.(3) we can get m and by setting $M(\hat{x}) = \hat{x}$ we can obtain the LBR value $\hat{x}$. Hence by reinjection probability density function can be described by Eq.(4) with $\lambda = \frac{1}{2}\frac{\alpha+1}{(c-\hat{x})^{\alpha+1}}$. For Fig.(5), we found that $m = 0.36$ and $m = 0.37$ for the lower and upper line respec-

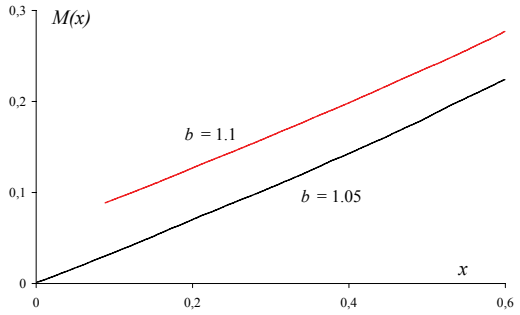

Figure 5: Numerical function $M(x)$ for the map (9). For the lower line $b = 1.05$ and for upper one $b = 1.1$. After numerical fitting, we have $m \approx 0.36$, $\hat{x} \approx 0$ and $m \approx 0.37$, $\hat{x} \approx 0.053$, respectively. The rest of the parameters used are $a = 1$ and $\varepsilon = 0.01$.

tively. Fig.(6) shows the RPD for the same cases plotted in Fig. (5). The continuous curve in this figure corresponds to the analytical expression given by Eq.(3). The agreement between the numerical and theoretical results is very good. We only used the values of $\hat{x}$ and m founded in Fig.(5). Moreover, as shown in Fig.(6), the theoretical RPD function provides a better description than the one given by the numerical data because of the unavoidable statistical fluctuations. It is important to emphasize that a LBR different from zero produces a gap around the unstable point in the Poincaré map as has been observed from earlier experiments [16]. The LBR appears in the function $\phi(x) = \lambda x^{\alpha}$ as a positive shift on the variable x. Also, negative values of x_i can also be possible for Eq.(4). Therefore, if $x_i < 0$, the RPD function can be described by two overlapping functions, each one having the form given by Eq.(4):

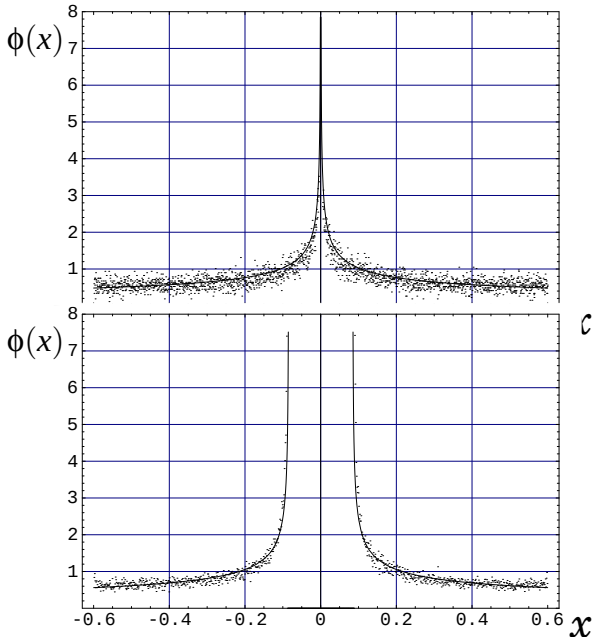

Figure 6: RPD for the same parameters used for Fig.(5). Dots are numerical data and continuous lines represent the Eq.(4).

$$\phi(x) = \begin{cases} \lambda\left[(|\hat{x}| + x)^{\alpha} + (|\hat{x}| - x)^{\alpha}\right] \text{ if } |x| \leqslant |\hat{x}| \\ \lambda\left(|\hat{x}| + x\right)^{\alpha} \text{ if } |\hat{x}| < x \leqslant c \\ \lambda\left(|\hat{x}| - x\right)^{\alpha} \text{ if } -c < x \leqslant -|\hat{x}| \end{cases} \tag{10}$$

where $\lambda > 0$ is again obtained by the normalization condition

$$\lambda = \frac{1}{2}\frac{\alpha + 1}{(c + |\hat{x}|)^{\alpha+1}} \tag{11}$$

The RPD given by Eq.(10) is also specified by the two

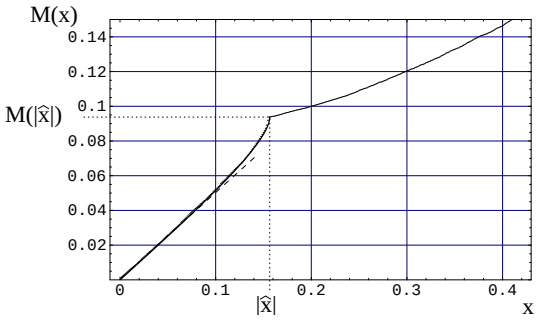

Figure 7: Numerical evaluation of $M(x)$. Singular point is $|\hat{x}| \approx 0.157$. The continuous line represents Eq.(12) for $x < |\hat{x}|$ and the dashed one is the straight line with slope 1/2. The parameters are $a = 1.035$, $b = 1.05$ and $\varepsilon = 0.001$.

parameters α and $\hat{x}$, as in the previous case. However, the function $M(x)$ is not linear in x because the reinjection is generated by superimposing two simultaneous processes (see Fig.7). The RPD given by Eq.(10) is non-continuous for $x = |\hat{x}|$, then $M(x)$ has no derivative at this point, and the point $\hat{x}$ is a singular point for both $M(x)$ and $\phi(x)$. To reach the expression for $M(x)$ we use Eqs.(3 and 10):

$$M(x) = \frac{(1+\alpha)\,x - |\hat{x}|}{(2+\alpha)} \left[\frac{|\hat{x}|\left(|\hat{x}| - x\right)^{1+\alpha} - |\hat{x}|^{2+\alpha}}{\left(|\hat{x}| - x\right)^{1+\alpha} - \left(|\hat{x}| + x\right)^{1+\alpha}}\right] \frac{2}{(2+\alpha)} \tag{12}$$

To obtain the value of α, we valuated the Eq.(12) in $x = |\hat{x}|$. The next step is to verify the assumptions made in obtaining the RPD in Eq.(10). To do this we compare numerical data for $M(x)$ with the Eq.(12). In

ISBN: 978-1-61804-131-9

Fig.(7) we plot both analytical and numerical M and we can observe a very good agreement. In Fig.(8) we compare the RPD function, Eq.(10), with the numerical data. The values of x_i and α have been calculated from the function $M(x)$ for the same parameters used in Fig.(7). Finally, we note that the overlapping of the new function $\phi(x)$ is clearly exhibited in the figures. Once the RPD function is calculated, we can evaluate

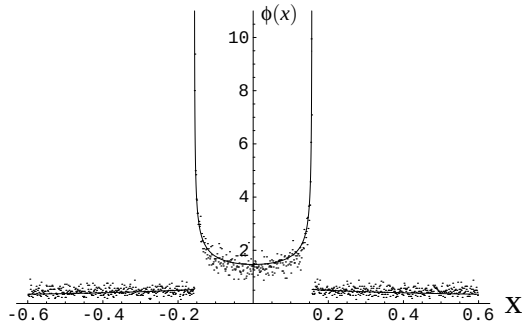

Figure 8: RPD for the same parameters used in Fig.(7). Dots are numerical data and continuous lines are referred Eq.(10).

the probability density of the laminar length $l(x,c)$

$$\phi_l(l) = 2\lambda \left(X(l,c) - \hat{x}\right)^{\alpha} \left[aX(l,c)^3 + \varepsilon X(l,c)\right] \tag{13}$$

where $X(l,c) = \sqrt{\frac{\varepsilon}{(a+\varepsilon/c^2)e^{2\varepsilon\, l} - a}}$. In Fig.(9) we show the comparison between numerical data for the probability of laminar phase length and the results calculated with Eq.(13). For Fig.(9) we use the same parameters $\hat{x}$ and m corresponding to lower and upper line respectively of Fig.(5). Note that in Fig.(9.a) the probability of laminar phase length values can be arbitrarily very large because of $\hat{x} \approx 0$. On the contrary, for $b = 1.1$, we have $\hat{x} > 0$ and this fact gives rise the existence of an upper cut-off value for $\hat{l}$ as shown in Fig.(9.b). For $x_i < 0$, by ussing Eqs.(10) and (13), the probability of laminar phase length is

$$\phi_l(l) = 2\lambda \left[(|\hat{x}| + X(l,c))^{\alpha} + +k\left(|\hat{x}| - X(l,c)\right)^{\alpha}\right] \left[aX(l,c)^3 + \varepsilon X(l,c)\right] \tag{14}$$

where $k = 0$ for $|l| \leqslant \left|\hat{l}\right|$ and $k = 1$ for $|l| > \left|\hat{l}\right|$. Fig.(10) shows the comparison between the numerical values and the Eq.(14). The parameters $\hat{x}$, α and λ used in this figure are the same that we used in Figs.(7 and 8). Fig.(10) has a mirrored form. When $\hat{x} > 0$ we find that $\hat{l}$ is a cut-off value, whereas for $\hat{x} < 0$ the function ϕ_l does not have a cut-off and this function continues to infinite. To the average laminar length and the characteristic relation considering $x_i < 0$, we established a more general result [11]: If the system

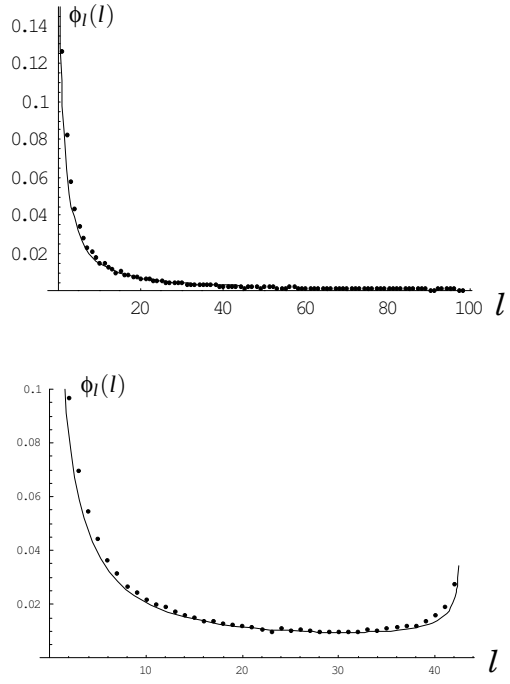

Figure 9: ϕ_l for the same test of Fig.(7). Eq.(13) is represented by lines.

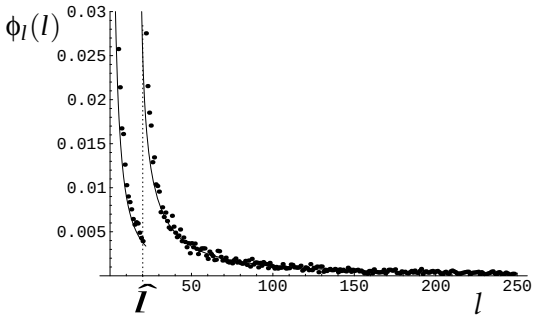

Figure 10: ϕ_l for the same test of Fig.(8). Eq.(14) is represented by lines.

verifies the following two assumptions: *i)* $\phi(0) \neq 0$ and *ii)* $\left.\frac{\mathrm{d}\phi(\mathrm{x})}{\mathrm{dx}}\right|_{x=0}$ is bounded, then the function $M(x)$ can be approximated, near of $x = 0$, as $M(x) = x/2$ hence its characteristic relation will be $\bar{l} \propto \varepsilon^{-0.5}$. This means that the uniform reinjection is not needed to get the value -0.5 as the critical exponent.

5 Noise influence

In this section we study the noise influence on the statistical properties of intermittency, and we follow the research published in [12]. It is clear that noise affects all system dynamic, therefore it will be affect the RPD function. We note that in the previos studies about of

the local noise effect is usually assumed that the noise strength σ is much smaller than ε. Here, we consider a general process where this hypothesis is not necessary. We apply our noisy theory to previous maps. For instance, for type-II intermittency we transfor the map (5) into the noisy map:

$$x'_{n+1} = \begin{cases} F(x_n) + \sigma\xi_n & x_n \leq x_r \\ (F(x_n) - 1)^\gamma + \sigma\xi_n & x_n > x_r, \end{cases} \quad (15)$$

ξ_n is a uniform distributed noise verifying that $< \xi_m, \xi_n >= \delta(m-n)$ and $< \xi_n >= 0$. The noise strength is given by σ. To keep x'_{n+1} in the unit interval we modifies the the map as follows:

$$x_{n+1} = \begin{cases} |x'_{n+1}| & x'_{n+1} \leq 1 \\ |x'_{n+1}| - 2\,\mathrm{mod}(|x'_{n+1}|, 1) & x'_{n+1} > 1. \end{cases} \quad (16)$$

We can note that when $\sigma = 0$, we recover the previ-

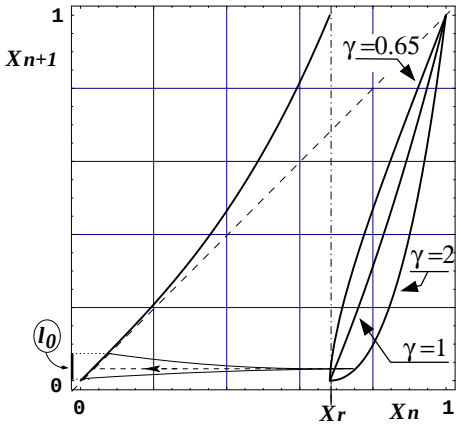

Figure 11: Map of Eqs.(15-16) with $\sigma = 0$ (hence it is equal to map (5)) and $\varepsilon = 10^{-3}$.

ously used map. Fig.(11) shows the reinjection mapping into the laminar region. The dashed arrow represents the noiseless trajectory. However, the trajectory for the system (15-16), due to the noise, may spread over a region enclosed by the solid lines. To analyze the noise influence in type-III intermittency, we use the following map:

$$x_{n+1} = -(1+\varepsilon)\, x_n - a\, x_n^3 + d\, x_n^6\, \sin(x_n) + \sigma\xi_n, \quad (17)$$

If we consider a noiseles case ($\sigma = 0$), we recover the map (9). As fist step we calculate the function $M(x)$ for the map (15-16) considering two cases: with and without noise. The results are indicated in Fig.(12). The functions $M(x)$ for noise and noiseles tests are smooth becuase the definition of $M(x)$ smoothed the data. For the noisy tests $M(x)$ has different bahavior on each side of x_c and it can be approximated by a piecewise linear function with two slopes. And the

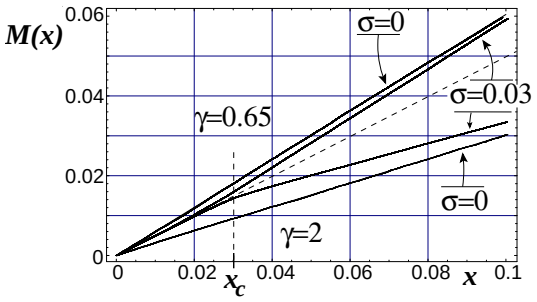

Figure 12: Numerical simulations of $M(x)$ for the map (15-16). The dashed line has slope $1/2$. The lines above the dashed one correspond to $\gamma = 0.65$. The same values of noise strength is used for the two lines below the dashed one, that correspond to $\gamma = 2$. For all the cases $\varepsilon = 0.001$ is fixed and $c = 0.1$.

value x_c depends on the noise intensity, σ. For $x < x_c$ the slope of $M(x)$ approaches $1/2$, as we expect for the uniform reinjection. However, for $x_c < x$, the slope of $M(x)$ reaches a very similar value to the corresponding noiseless slope. For $\gamma = 0.65$ in the noisy test the slope is $m \approx 0.61$ and to the noiseless case $m \approx 0.60$. Then, in the region $x_c < x$ the noisy RPD (NRPD) must have a similar form that the RPD function. This is a very important property of $M(x)$ because by means of the noisy data analysis we can obtain the RPD function for the noiseless case. We note that noise acts on the complete system. However, it does not afects the function $M(x)$ in the region $x > x_c$. Then, on the right side of x_c, the RPD function is robust against the noise but in the region $x < x_c$ the noise modifies the RPD. The noise influence, for $x < x_c$, produces that the RPD aproaches to the uniform reinjection, at least locally around $x = 0$. For type-III intermittency, we find a similar behavior. The main difference happens in the value of x_c, that in this case it is bigger. We start with a numerical calculation of the function $M(x)$. The results are ploted in Fig.(13). We note that for values close to the origin (on the left of the arrows), the function $M(x)$ approaches $M(x) \approx 0.5x$, but for points on the right hand side of the arrows we have $M(x) \approx mx$ where the slope m is similar as to in the noiseless map. For the map with type-III intermittency the effect of noise on the function $M(x)$ is stronger than for the map with type-II intermittency because the transition from the 0.5 slope to a slope close to the noiseless test takes place for bigger values of x_c than for the type-II map.

5.1 NRPD in type II intermittency

To obtain an analytical expression for the NRPD, denoted by $\Phi(x)$, we analyse the effect of noise on the reinjection trajectories, as it is described in Fig.(11).

ISBN: 978-1-61804-131-9

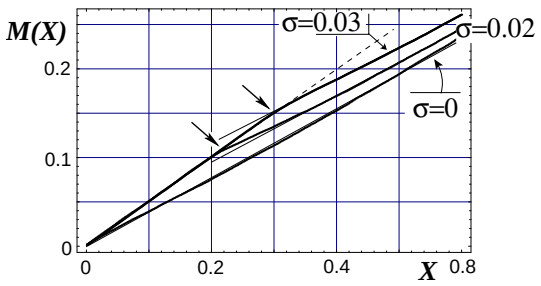

Figure 13: Function $M(x)$ for the map Eq.(17). The parameters are: $c = 0.8$, $a = 1.1$, $d = 1.35$, $\varepsilon = 10^{-4}$. Arrows show when $M(x)$ change the $1/2$ slope.

A trajectory withouth noise is indicated by a dashed line, when this trajectory is perturbed by noise the reinjection point can be palced inside of the interval l_0. That is, the noiseless density $\phi'(x)$ should be transformed into a new density $\Phi(x)$ according to the convolution: $\Phi(x) = \int \phi'(y)G(x-y,\sigma)dy$. Where $G(x,\sigma)$ is the probability density of the noise term $\sigma\xi_n$ in Eq.(15). For $x > x_c$, the slope of the noisy $M(x)$ approaches the corresponding slope without noise, and we can calculate the function $\phi(x)$ without noise. These developments suggest that $\phi'(x) \approx \phi(x)$, where $\phi(x) = \lambda|x|^\alpha$ is the noiseless RPD. We note that the parameters λ and α are the values for the noiseless map. We introduce $\phi'(x) = \lambda|x|^\alpha$ in the convolution integral to prove this assumption. As noise source we used a random variable ξ in the interval [-1,1], hence its probability density G in Eq.(15) and (17) is given by $G(x,\sigma) = \frac{\Theta(x+\sigma)-\Theta(x-\sigma)}{2\sigma}$. Where $\Theta(x)$ is the Heaviside step function. After solving the integral, we can writte the NRPD function as:

$$\Phi(x) = \frac{1}{c^{1+\alpha}} \frac{(|x|+\sigma)^{1+\alpha} - Sg(|x|-\sigma)||x|-\sigma|^{1+\alpha}}{2\sigma}, \tag{18}$$

$Sg(x)$ is the sign function. In Fig.(14) we compare the results calculated by Eq.(18) with the numerical simulations for different noise levels. We consider the same values of m and α obtained from Fig.(12). We observe a good agreement between the numerical simulations and the analytical evaluations. However, when the intensity of the noise is higher we find differences of about 10 percent between the noiseles slopes m obtained with and without noise data. But, the power law exponential form of the RPD, $\phi'(x) = \lambda|x|^\alpha$, remains robust [12].

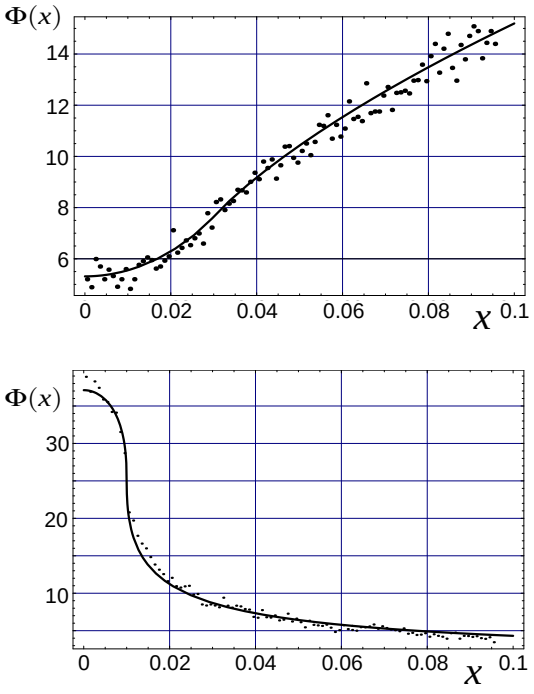

Figure 14: NRPD for the map Eq. (15-16). a) $c = 0.1$, $\gamma = 0.65$, $\sigma = 0.03$ and b) $c = 0.1$, $\gamma = 2$ and $\sigma = 0.01$. Dots correspond to numerical data, Eq.(18) is plotted as a solid line.

5.2 NRPD in type III intermittency

We show in the previous section that the noiseless RPD for type-III intermittency follows a power law. This law depends on the neighboring points of the map maximum and minimum values, Eq.(17), [11]. In Fig.(15), we indicate using a dashed line the noiseless trajectory of a point starting near the maximum value of the map. When the noise affects the system, this trajectory may spread over a region of some width, denoted here by l_0. We can observe that l_0 will be stretched on the graph of the map by a suitable factor K, $l_1 = Kl_0$. The factor K depends of the particular form of the map. To reach an analytical equation for $\Phi(x)$, we consider that the map Eq.(17) can be represented by a composition of the two maps: one of them corresponds to a noiseless map $x'_n = -(1+\varepsilon)\ x_n - a\ x_n^3 + d\ x_n^6\ \sin(x_n)$, and the another is a new map $x_{n+1} = x'_n + \sigma\xi_n$ We use here a similar argument that for type-II intermittency, and we consider that $\rho'(x)$ is the invariant density in a region close to the maximum of the map without noise. Then, the noise influence on this density can be obtained by means of the convolution $\rho(x) = \int \rho'(\tau)G(\tau - x,\sigma)d\tau$, where $\rho(x)$ is the invariant density in the interval l_0. Unlike to the analized type-II intermittency test, for this type-III intermittency map, points placed on l_0 are not directly

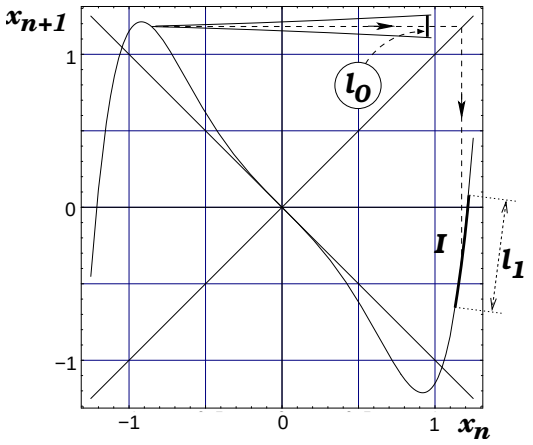

Figure 15: Map of Eq.(17). Dashed line indicates the effect of the map on a point near the maximum. Solid lines represent the noise effect on the same point.

mapped on the laminar region. Therefore to obtain the NRPD, we must follow the evolution of the density $\rho(x)$ produced by the map (17) [12]:

$$\Phi(x) = \frac{1}{c^{1+\alpha}} \frac{(|x| + K\,\sigma)^{1+\alpha} - Sg(|x| - K\,\sigma)||x|}{2K\,\sigma} - \frac{K\,\sigma|^{1+\alpha}}{(2K\,\sigma)c^{1+\alpha}} \tag{19}$$

This expression is plotted in Fig.(16) showing agreement with the numerical results.

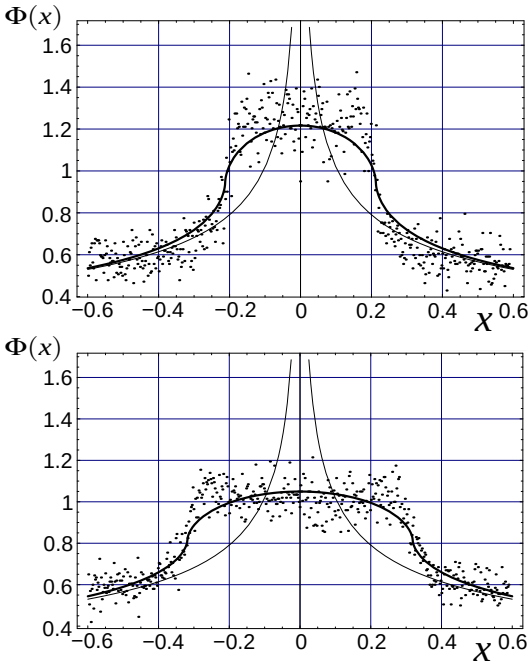

Figure 16: NRPD for two values of the noise strength σ of the Eq.(17): a) $\sigma = 0.02$ and b) $\sigma = 0.03$. Dots are numerical data whereas solid lines are given by Eq.(19). The noiseless RPD is also plotted. The parameters are:$c = 0.6$, $a = 1.1$, $d = 1.35$, $\varepsilon = 10^{-4}$.

6 Conclusion

In this paper we have presented a review of a new formulation of intermittency theory. We have applied this formulation to type-II and type-III intermittency with and without noise effects [10, 11, 12]. We have introduced a new RPD function for a broad class of systems. To achieve this we have used the function $M(x)$ which is easy to calculate. We have found that the function $M(x)$ has a linear form. By means of a numerical evaluation of the function $M(x)$, we have obtained the values of the parameters m and $\hat{x}$. With only theses two parameters, we provide a whole description of the RPD. Once we obtained the RPD function, we established analytical relations for the probability of the laminar length, the average length, and the characteristic relations. In all tests performed, the numerical data and theoretical results have shown a very good agreement. When $\hat{x} > 0$, the system has a LBR and there is a cut-off value for the laminar phase length. For $\hat{x} < 0$ the system has a more complex RPD which is a linear combination of RPD describing the case of $\hat{x} > 0$. This behavior modified the linearity of the function $M(x)$. However, even in theses test, the function $M(x)$ provides us enough information to completely determine the function $\phi(x)$. Finally, we have investigated the noise effect on the RPD function. We have found that the new methodology developed to describe the noiseles reinjection is robust against noise. Then, we can use the RPD to obtain an analytical description of the NRPD in accordance with numerical simulations. For the other hand, we note that from the NRPD, obtained from noisy data, we have a complete description of the noiseless system.

Acknowledgements: This paper was supported by grants of CONICET, UPM, UNC, MCyT-Córdoba.

References:

[1] P. Manneville and Y. Pomeau, *Phys. Lett.A*, 75, 1979, pp.1-2

[2] Y. Pomeau and P. Manneville, *Comm. in Math. Phys.*, 74, 1980, pp.189-197.

[3] J. Zebrowski and R. Baranowski, *Physica A*, 336, 2004, pp.74-83

[4] A. Chian, *Complex Systems Approach to Economic Dynamics*, Springer, Berlin, 2007.

[5] H. Schuster and J. Wolfram, *Deterministic Chaos*, WILEY-VCH Verlag GmbH & Co. KGaA, Weinheim, 2005.

[6] A. Nayfeh and B. Balachandran, *Applied Nonlinear Dynamics*, John Wiley & Sons Inc., New York, 1995.

[7] S. Wiggins, *Introduction to Applied Nonlinear Dynamical Systems and Chaos*, Springer-Verlag, New York, 1990.

[8] W. Kye and C. Kim, *Phys. Rev. E*, 62, 2000, pp. 6304-6307.

[9] W. Kye et al., *Phys. Rev. E*, 68, 2003, 036203.

[10] E. del Rio and S. Elaskar, *Int. J. Bifurcation and Chaos*, 20, 2010, pp.1185-1191.

[11] S. Elaskar, E. del Rio, and J. Donoso, *Physica A*, 390, 2011, pp.2759-2768.

[12] E. del Rio, M. Sanjuan and S. Elaskar, *Com. Non. Scs. Num Simulation*, 17, 2012, pp.3587-3596

[13] P. Manneville, *Le Journal de Physique*, 41, 1980, pp.1235-1243.

[14] J. Laugesen, N. Carlsson, E. Mosckilde and B. Bountis, *Open System & Information Dynamics*, 4, 1997, pp.393-405.

[15] C. Kim, G. Yim, Y. Kim, J. Kim and H. Lee, *Phys. Rev. E*, 56, 1997, pp.2573-2577.

[16] M. Dubois, M. Rubio O. and Berge, *Phys. Rev. Lett.*, 51, 1983, pp.1446-1449.